water

MDPI

Article

An Improved Configuration of Vertical-Flow Mesh Tube Filters for Seawater Pretreatment: Performance, Cleaning, and Energy Consumption

Dong-Ho Kim [1], Changkyoo Choi [2], Chulmin Lee [1], Rusnang Syamsul Adha [1], Thanh-Tin Nguyen [1], Sang-Jun Ahn [3], Hee-Jong Son [4] and In S. Kim [1,*]

1 Global Desalination Research Center (GDRC), School of Earth Sciences and Environmental Engineering, Gwangju Institute of Science and Technology (GIST), Gwangju 61005, Korea; dhowon16@gist.ac.kr (D.-H.K.); min90821@gist.ac.kr (C.L.); rusnangadha@gist.ac.kr (R.S.A.); nguyenthanhtin@gist.ac.kr (T.-T.N.)
2 Water Convergence Research Team, Department of Water Industry Promotion, Korea Water Cluster, Korea Environment Corporation, Daegu 43008, Korea; simonchoi@keco.or.kr
3 KEOSONG Research Institute, KEOSONG Construction Co., Ltd., Seoul 06640, Korea; blueload17@naver.com
4 Water Quality Institute, Water Authority Busan, Gimhae, Gyeongnam 50804, Korea; menuturk@hanmail.net
* Correspondence: iskim@gist.ac.kr

Received: 31 August 2020; Accepted: 6 October 2020; Published: 10 October 2020

Abstract: Roughing filters are types of porous media filter used in pretreatment systems where the raw water contains a large amount of suspended particles (SPs) and organic matter. Mesh tube filtration (MTF) media are roughing-filter media composed of low-density polyethylene used for SP removal during wastewater treatment. In this study, we present an improved MTF design—a porous filter bed (PFB), which exhibits superior SP removal performance compared to conventional MTF media. We then compare the applicability of MTF and PFB to both the primary pretreatment process for seawater desalination and the water reuse process. In bench-scale SP removal experiments, PFB shows removal rates of 46.7%, 68.0%, 67.6%, and 68.4% at hydraulic retention times of 15, 20, 30, and 60 min, respectively, which are better than those of MTF. The specific energy consumption (SEC) of batch dissolved air flotation (DAF) was known to range from 0.035 to 0.047 kWh/m^3, whereas the SEC calculated for pilot-scale MTF and PFB is 0.027 kWh/m^3 and minimum energy for influent supply, respectively. This suggests that PFB can compete with DAF as a primary pretreatment process. MTF predominantly removes SPs by sedimentation, whereas SP removal in PFB typically occurs via deposition of SPs on the mesh tube media.

Keywords: suspended particles; roughing filters; mesh tube filtration; porous filter bed; specific energy consumption

1. Introduction

Seawater contains a variety of dissolved and colloidal foulants (iron, manganese, silica, etc.) and natural organic matter (NOM) that are difficult and costly to remove [1,2]. Therefore, pretreatment processes are essential to remove any suspended particles (SPs) in seawater and protect the membrane systems of seawater desalination plants; such processes include microfiltration (MF), ultra-filtration (UF) and reverse osmosis (RO) [3].

Porous media filtration is a water treatment process that has long been used to effectively remove SPs from water [4,5]. Generally, filtration methods include slow sand filtration and roughing filtration [4]. Slow sand filters effectively remove SPs and do not require chemicals or electrical

energy for operation; however, these filters need to lower the turbidity of the influent to operate efficiently. Therefore, under conditions of high microbial activity in summer and when the raw water is turbid, filter blockage due to bio-clogging will occur more quickly, necessitating pretreatment [6] and preventing the effective use of ordinary sand filters [4]. Thus roughing filters are commonly used as pretreatment systems prior to sand filtration [7]. The larger the filter media particles, the higher the controlled filtration rate, the smaller the media particles, and the greater the SP removal performance of the filter.

In 2010, a Korean environmental equipment company developed a rough filter process using low-density polyethylene (LDPE) filter media to remove high-concentration SPs and dissolved phosphorus during wastewater treatment [8,9]. Mesh tube filtration (MTF) media are classified as roughing filter media due to their cylindrical shape with a length of 25 mm and diameter of 5 mm. The zeta potential of MTF media is converted from negative to positive at the high ionic strength of seawater; therefore, SPs in seawater are effectively deposited on the surface of the MTF media. As such, the MTF process is expected to be useful in the primary pretreatment of seawater desalination. In a recent study, the performance of MTF and dissolved air flotation (DAF) was compared and analyzed, including for energy consumption, microalgal cell removal rate, and algal organic matter (AOM) removal rate [10]. When the DAF was operated at the level of energy consumption equivalent to MTF, DAF's microalgae removal performance was significantly lower than that of MTF. The maximum removal values for turbidity and microalgal cells in DAF were 70.3% and 77.3%, respectively. These observations suggest that MTF is more energy efficient than DAF for the seawater RO desalination of harmful algal blooms. Moreover, DAF achieved higher removal of AOM than MTF. However, the design of conventional horizontal MTF has not yet been optimized; thus, in order to use MTF as the primary pretreatment process in seawater desalination plants for more efficient high-concentration SP removal, an optimized reactor-tank design is required for performance improvement.

Roughing filters are also divided into vertical-flow and horizontal-flow types according to the water flow in the filter media, with vertical-flow types divided into up-flow and down-flow types [4,11]. In general, the horizontal-flow type can freely adjust the depth of the medium, resulting in the most efficient SP removal and enabling filtration at higher flow rate conditions [4,11]. However, horizontal-flow roughing filters have disadvantages such as low clean-in-place (CIP) process efficiency and a complicated facility design for backwashing [5].

In this study, we propose a new vertical-flow roughing filter configuration with the aim of improving the performance of conventional MTF. The new MTF design is based on a porous filter bed (PFB). Moreover, we compare the performance of the two filters (MTF and PFB) as a function of particle size, flow rate, and influent ion strength. The two filters are operated continuously for 72 h using the blended influent of natural seawater and secondary treated wastewater effluent and their performance is compared. The treated water of the filters and the rinsed water of the MTF media are analyzed by liquid chromatography–organic carbon detection (LC–OCD) to characterize the contaminants. The goal of this study is to develop a roughing filter configuration that achieves a more efficient primary pretreatment for seawater desalination using MTF media.

2. Materials and Methods

2.1. MTF Media

For SP removal during wastewater treatment, we used MTF media consisting of synthetic textiles and LDPE provided by KEOSONG Construction Co., Ltd. (Goyang-si, Gyeonggi-do, Korea) [9]. The length of the mesh tube is 25 mm and the diameter is 5 mm. A net of rhombus grids makes up the wall of the tube, with several strands of cilia at each end of the tube. The net size of the rhombus lattices is 0.75 × 0.85 mm and the bulk density and density of the packed tubes are approximately 0.06 g/cm^3 and 520 ea/L, respectively. The porosity of the filter bed filled with the mesh tube filter media is approximately 0.896 (±0.005) [9]. Photographic images of the filter media are shown in Figure 1.

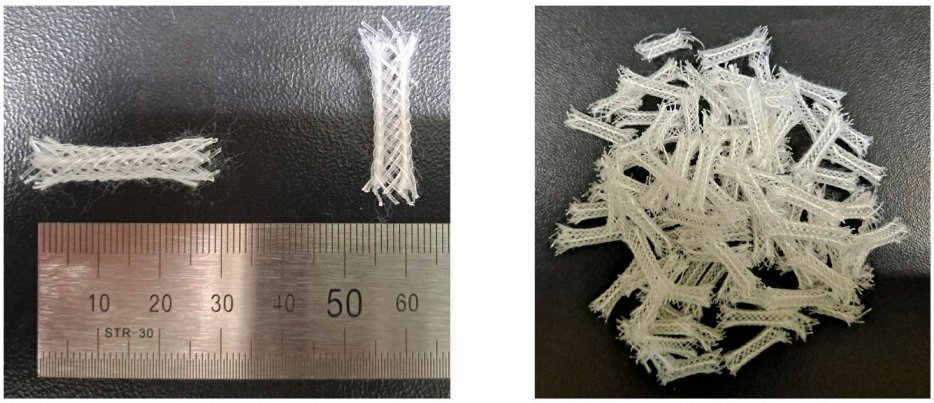

Figure 1. Photographs of the mesh tube filter media employed in this study.

2.2. Characterization of Suspended Particles (SPs)

Kaolin particles (Daejung Chemicals & Metals, Siheung, Korea) were used as injection SP, whereas kaolin particles and three types of silica (SiO_2) particles (US Research Nano Materials, Houston, TX, USA) were used for the analysis of the Derjaguin, Landau, Verwey, and Overbeek (DLVO) interaction energy between SPs and the filter media. Prior to their use as SPs in the experiment, the size of each particle material was analyzed using a particle size analyzer (N5 submicron particle size analyzer, Beckman Coulter, Brea, CA, USA). The analysis showed that the size of the kaolin particles was predominantly between 0.5 μm and 40 μm, with a median diameter (d_{50}) of 7.4 μm. The SP sizes of the three types of silica particles were 0.8 μm, 10 μm, and 20 μm, respectively, with ranges from 0.5 μm to 5.9 μm with d_{50} = 1.5 μm, from 4.5 μm to 15.8 μm with d_{50} = 10.4 μm, and from 6.7 μm to 32.8 μm with d_{50} = 19.5 μm, respectively. The size distribution data of each type of suspended particle is the same as the data presented in the paper (Figure 2) previously published [9]. A zeta potential analyzer (ELS-8000, Otsuka, Japan) was used to measure the zeta potential of the SPs and a flat sheet of LDPE (the material used in the MTF media).

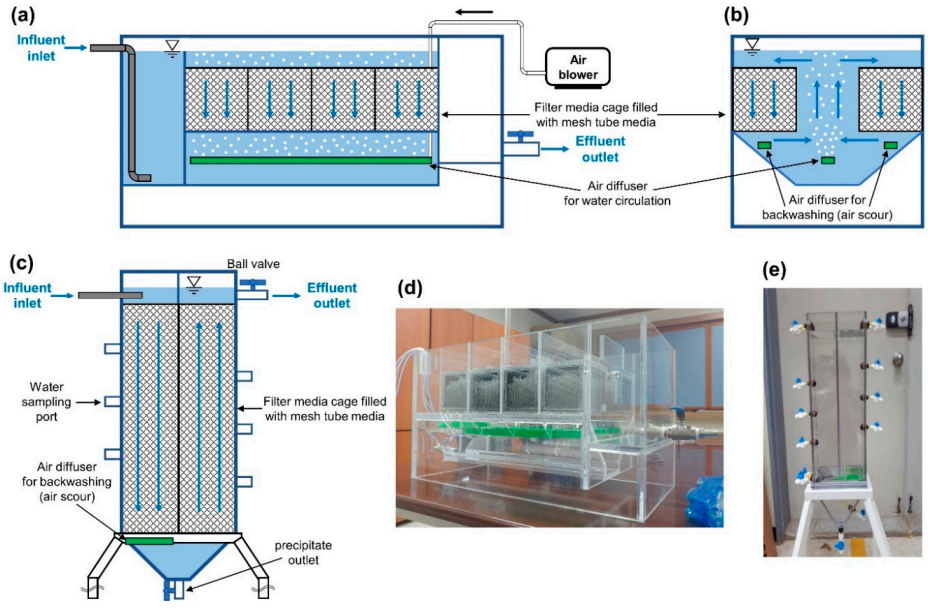

Figure 2. Cross-sectional diagram and photographs of two types of vertical-flow roughing filter: (**a**) mesh tube filter (MTF) section in the direction of water flow, (**b**) MTF cross-section in the direction perpendicular to water flow, (**c**) porous filter bed (PFB) section in the direction of water flow, (**d**) photograph of MTF reactor, (**e**) photograph of PFB reactor.

2.3. Suspended Particle Filtration Experiments

To compare the filter performance of MTF and PFB, bench-scale MTF and PFB reactors made of poly (methyl methacrylate) were fabricated. The working volume of the bench-scale MTF reactor was approximately 28 L and the overall size of the reactor was approximately 300 mm (w) × 600 mm (d) × 200 mm (h). The working volume of the bench-scale PFB reactor was approximately 12 L and the dimensions were approximately 200 mm (w) × 100 mm (d) × 800 mm (h) (excluding the pedestal) (Figure 2). The reactors were fed by a reservoir containing artificial seawater at pH 6.1 ± 0.2. The composition of the artificial seawater was based on ASTM D1141-98, with slight modifications (Table 1). The feed water was supplied to the reactors using gear pumps (Masterflex Digital Gear Pump 75211-70, Cole-Parmer, Vernon Hills, IL, USA) and variable area flow meters (GY-32461-40, Cole-Parmer, Vernon Hills, IL, USA) installed at the column inlet to measure the flow rate. A schematic diagram of the experimental set-up is shown in Figure 3

Table 1. Artificial seawater composition.

Salt (g)	g/L
NaCl	24.530
$MgCl_2$	5.200
Na_2SO_4	4.090
$CaCl_2$	1.160
KCl	0.695
$NaHCO_3$	0.201
KBr	0.101
H_3BO_3	0.027
Total salt mass (g)	36.004
Solution density (g/L)	

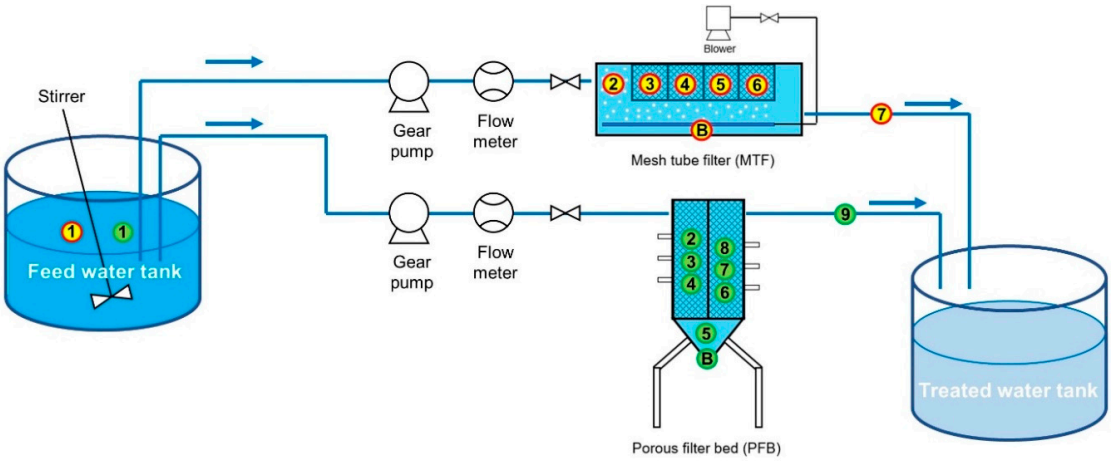

Figure 3. Schematic diagram of the experimental set-up. (The numbers in the figure refer to the sampling points, the numbers in the red circle indicate the MTF sampling points, and the numbers in the green circle indicate the PFB sampling points.).

2.4. DLVO Interaction Energy Calculation

In an electrolyte solution, suspended particles are affected by the attractive or repulsive interaction energies as they approach the solid–water interface. The DLVO theory considers that the interaction energy is generated due to the superposition of the electric attraction and repulsive force between two particles. Other non-DLVO interactions may occur due to Born repulsion, hydration and hydrophobic forces, and steric interactions [12]. In this study, the total interaction energy Φ for a particle and

collector system was considered to be the sum of electrostatic (Φ_{EDL}), van der Waals (Φ_{VDW}), and Born (Φ_{BORN}) repulsion interaction energies [9,13]:

$$\Phi(\delta) = \Phi_{EDL}(\delta) + \Phi_{VDW} + \Phi_{BORN}(\delta) \quad (1)$$

The total interaction energy Φ was calculated by modeling the SP–sand grain system as a sphere–plate interaction. Repulsive electrostatic double-layer interaction energies were calculated using the following expression [13,14]:

$$\Phi_{EDL}(\delta) = \varepsilon_0 \varepsilon_r \cdot \pi \frac{d_p}{2} \left(2\zeta_g \zeta_p \ln\left(\frac{1 + e^{-\kappa_d \delta}}{1 - e^{-\kappa_d \delta}} \right) + \left(\zeta_g^2 + \zeta_p^2 \right) \ln\left(1 - e^{-2\kappa_d \delta} \right) \right) \quad (2)$$

where ε_0 is the dielectric permittivity in a vacuum (8.854×10^{-12} F/m), ε_r is the relative dielectric permittivity of water (equal to 78.4 for water at 20 °C), δ is the separation distance between the SP and sand grain surface, d_p is the SP diameter, and κd is the Debye length (κd^{-1} is the characteristic thickness of the diffuse layer of charge). For water at 20 °C, κd^{-1} is equal to 3×10^{-10} (IS)$^{-0.5}$ m [15], where IS denotes the ion strength in mols per liter. ζ_p and ζ_g are the zeta potentials of SPs and sand grains, respectively.

The van der Waals attractive interaction energy was calculated as follows [13,16]:

$$\Phi_{VDW}(\delta) = -\frac{A}{12} \left(\frac{d_p}{\delta} + \frac{d_p}{\left(d_p + \delta \right)} + 2 \ln\left(\frac{\delta}{d_p + \delta} \right) \right) \quad (3)$$

where A is the Hamaker constant of the interacting media (SP–water–sand). A value of 10^{-20} J was employed for the Hamaker constant (inorganic particles) [17]. The Born repulsion, Φ_{BORN}, was calculated from [18] as follows:

$$\Phi_{BORN}(\delta) = \frac{A \sigma_p^6}{7560} \left(\frac{4d_p + \delta}{\left(d_p + \delta \right)^7} + \frac{3d_p - \delta}{\delta^7} \right) \quad (4)$$

where σ_p is the collision diameter and typically assumed to equal 0.5 nm [12,13,19,20]. The DLVO interaction energy profiles for SPs were then calculated using the measured zeta potentials at different ionic strengths. Interaction energies are commonly made dimensionless by dividing them by the product of the Boltzmann constant ($k_B = 1.38 \times 10^{-23}$ JK^{-1}) and the absolute temperature T (K) [9].

2.5. Computational Fluid Dynamics (CFD) Modeling of MTF and PFB for Specific Energy Consumption (SEC) Calculation

Fluid behavior is very difficult to predict because of the numerous variables [21]. However, computational fluid dynamics (CFD) tools are useful software for predicting fluid flows that are actively used in industry and research [22]. In this study, ANSYS CFX (version 19.1) was used to simulate the fluid behavior and transport of bovine serum albumin (BSA) particles. The governing equation of ANSYS CFX is the Navier–Stokes equation, which describes conservation and transport processes [21]. In this equation, the fluid is assumed to be Newtonian when the flow is steady and laminar (Equation (1)) [23].

$$\frac{\partial u}{\partial x} + \frac{\partial v}{\partial y} + \frac{\partial w}{\partial z} = 0 \quad (5)$$

Here, u is the velocity in the x direction, v is the velocity in the y direction, and w is the velocity in the z direction. The K–epsilon (k–ε) model is commonly adopted to interpret flow properties under turbulent conditions in CFD [21]. The model has two variables: turbulent kinetic energy (k) and the dissipation rate of turbulent energy (ε). The turbulent viscosity is considered isotropic where the ratio

between Reynolds stress and deformation rate, t, is the same in all directions [24]. The k–ε equations contain multiple unknown terms. As a practical approach, the standard k–ε model has been employed to minimize the unknown factor in many turbulence applications. The equations for turbulent kinetic energy (k) and dissipation (ε) are described as follows [25]:

$$k: \frac{\partial(\rho k)}{\partial t} + \frac{\partial(\rho k u_i)}{\partial x_i} = \frac{\partial}{\partial x_j}\left[\frac{\mu_t}{\sigma_k}\frac{\partial k}{\partial x_j}\right] + 2\mu_t E_{ij}E_{ij} - \rho\varepsilon \quad (6)$$

$$\varepsilon: \frac{\partial(\rho \varepsilon)}{\partial t} + \frac{\partial(\rho \varepsilon u_i)}{\partial x_i} = \frac{\partial}{\partial x_j}\left[\frac{\mu_t}{\sigma_\varepsilon}\frac{\partial \varepsilon}{\partial x_j}\right] + C_{1\varepsilon}2\mu_t E_{ij}E_{ij} - C_{2\varepsilon}\rho\frac{\varepsilon^2}{k} \quad (7)$$

where u_i is the velocity component in the corresponding direction, E_{ij} is the component of deformation rate, and μ_t is the eddy viscosity.

Simulations in this study were conducted using the three-dimensional finite-element method (FEM). In the CFD, the inlet and outlet were set based on the flowrate, pressure, and velocity. The flow rate of the MTF and PFB influent was set to 4.16 L/s (=360 m^3/d), and the influent water condition was a 1% concentration of BSA particles (density: 1.003 g/cm^3, viscosity: 1000 Pa·s). The volume of the filter bed of MTF was 3.2 m^3 (0.45 m (w) × 0.55 m (d) × 1.3 m (h) × 10ea), the volume of the filter bed of PFB was 3.3 m^3 (0.6 m (w) × 1.4 m (d) × 2 m (h) × 2ea), and the porosity of the filter bed filled with mesh tube media was set to 0.9. The detailed conditions of the inflow are shown in Table 2. The wall boundary conditions were applied under non-slip conditions.

Table 2. Analytical conditions of MTF and PFB using computational fluid dynamics (CFD) software.

Item	Value
Software	Ansys 19.1 CFX
Filter bed (MTF)	Volume: 3.2 m^3 (0.45 m (w) × 0.55 m (d) × 1.3 m (h) × 10ea) Porosity: 0.9 Aeration rate: 50 L/min using 10 air diffusers
Filter bed (PFB)	Volume: 3.3 m^3 (0.6 m (w) × 1.4 m (d) × 2 m (h) × 2ea) Porosity: 0.9
Inlet	Flow rate: 4.16 kg/s (≒ 360 m^3/d, HRT: 30 min) SS: 1% BSA (density: 1.003 g/cm^3, viscosity: 1000 Pa·s)

2.6. Field Experiments Using Natural Seawater and Secondary Wastewater Effluent

In order to determine the applicability of the water reuse process, comparison experiments of MTF and PFB performance were conducted using blended influent water of natural seawater and secondary treated wastewater. Natural seawater was collected from the offshore of Yeosu wastewater treatment plant (34.73 N, 127.68 E, Yeosu city, Jeollanamdo, Korea) and secondary wastewater effluent was collected from the Yeosu wastewater treatment plant. Both seawater and sewage have very low total suspended solids (TSS), so kaolin particles were periodically added to the influent reservoir to adjust the TSS concentration of the influent to 20 mg/L. The MTF and PFB reactors for SP removal were operated for 72 h and the change in SP concentration was monitored by analyzing the TSS concentration of the influent and treated water during this time. Changes in temperature, pH, and total dissolved solids (TDS) of the natural seawater and secondary treated wastewater during operation are shown in Figure 4. At 72 h after the start of operation, air scouring-based backwashing was performed to remove SPs deposited on the mesh tube media in both MTF and PFB reactors.

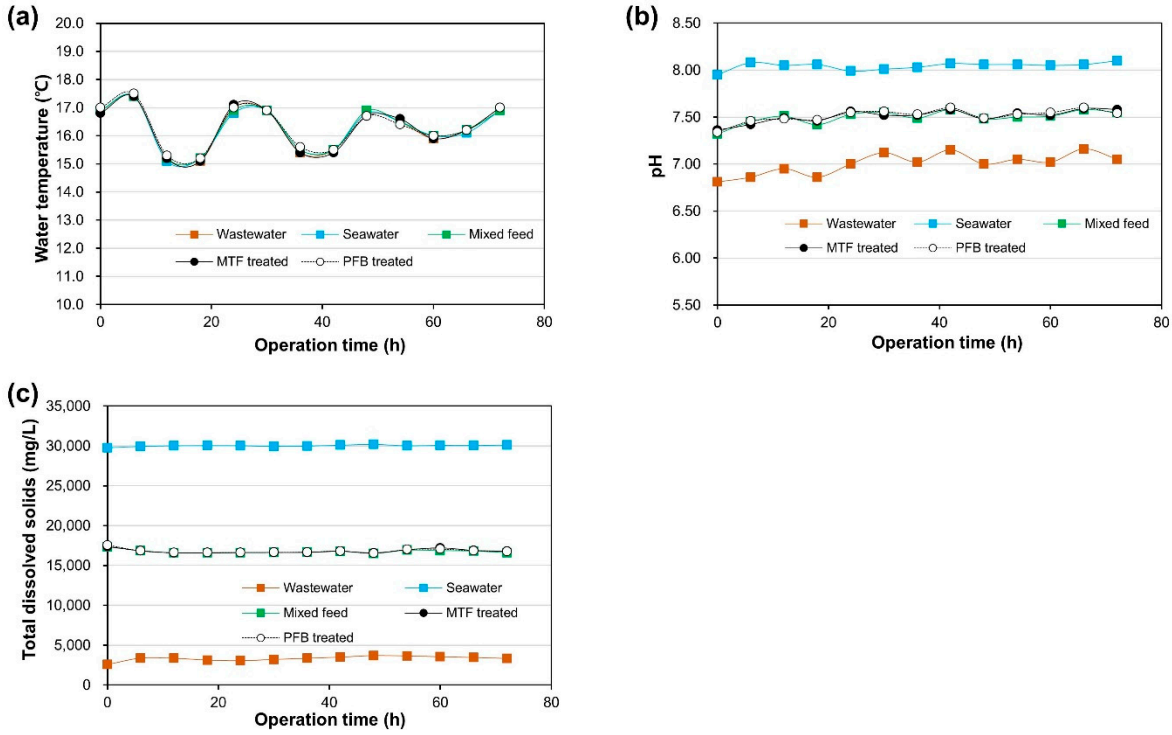

Figure 4. Characteristics of influent water during MTF and PFB field experiments (November 2019): (**a**) influent water temperature, (**b**) influent water pH, and (**c**) influent water total dissolved solids (TDS).

2.7. Organic Suspended Matter Analysis Using LC–OCD

LC–OCD is a fractionation method based on size exclusion chromatography coupled with different online analyzers such as organic carbon detection (OCD) and UV absorbance at 254 nm. According to previous literature, these facilitate the distribution of organic matter over the following five fractions: (1) biopolymers composed of polysaccharides and proteins, (2) humics (and fulvics), (3) building blocks that correspond to the breakdown products of humics, (4) low-molecular-weight (LMW) organic acids, and (5) LMW neutrals (alcohols, aldehydes, ketones, and amino acids) [26]. In order to assess the performance of the different treatments, LC–OCD analysis was performed on raw seawater, secondary treated wastewater, blended influent water, MTF-treated water, PFB-treated water, and mesh tube media (MTF and PFB) rinsing water.

3. Results and Discussion

3.1. Fluid Flow Analysis of Two Vertical-Flow Roughing Filters

The horizontal- and vertical-flow roughing filters show no significant difference in performance; however, due to structural constraints, it is difficult to use a long filter depth with vertical-flow roughing filters (Figure 5) [4]. In order to use vertical-flow roughing filters with very large depth, it is necessary to construct high vertical reactors, which are very difficult to maintain due to the need to clean and replace the filter media. However, in the floc of SPs deposited on the horizontal-flow roughing filter media, the particles sink to the bottom of the filter bed under the influence of gravity after floc aggregation; therefore, it is difficult to use a horizontal-flow roughing filter in coarse media filters such as MTF beds. Considering these characteristics, existing mesh tube filters are the down-flow type with a corridor of empty space placed in the center of the filter reactor, as well as powerful air aeration devices installed at the bottom of the empty space to produce air bubbles for water circulation inside the filter bed (Figure 2a,b) [8,10]. However, the current MTF structure has not been verified as an optimized mesh tube filter bed structure, and various types of filter bed designs have been devised

to improve the performance of the filter bed. In order to improve the performance of the conventional MTF, a new type of MTF, which is named porous filter bed (PFB) design, was devised to effectively remove SPs in the water by allowing water to evenly pass through the mesh tube media filter bed and reduce energy consumption by removing the aeration device (Figure 2c).

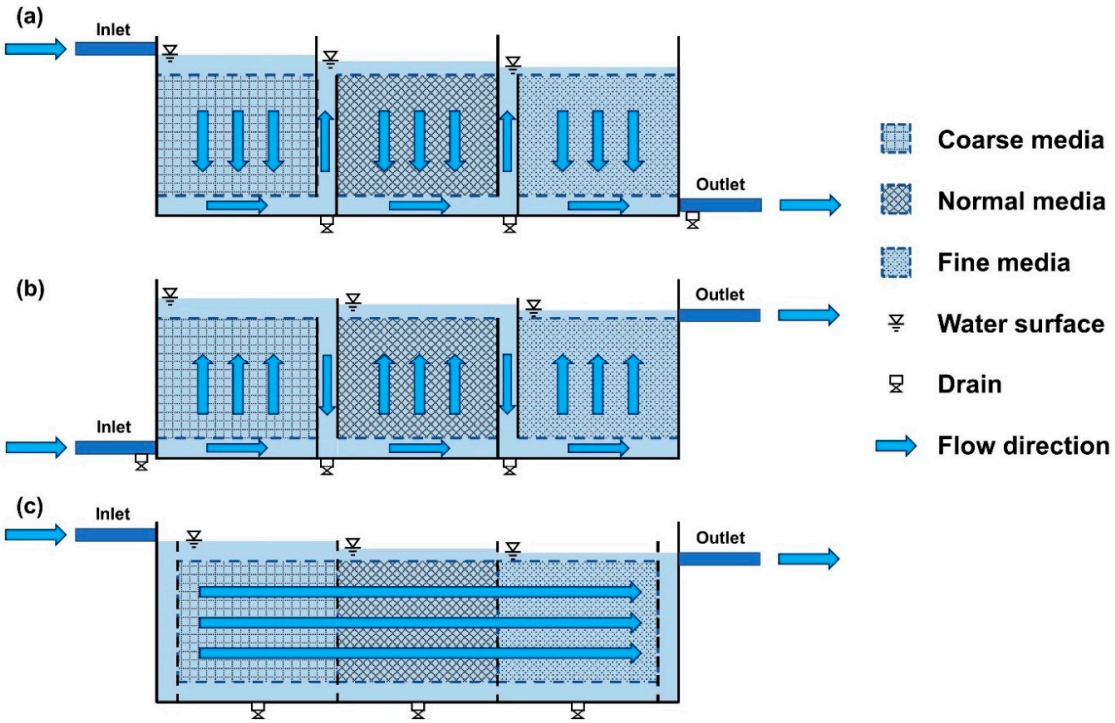

Figure 5. Schematics of horizontal and vertical roughing filters: (**a**) down-flow roughing filter, (**b**) up-flow roughing filter, and (**c**) horizontal-flow roughing filter [4,5,11].

3.2. Comparison of SP Removal Performance for Bench-Scale MTF and PFB Reactors

Prior to conducting experiments comparing the filter performance of bench-scale MTF and PFB reactors, SP removal tests were performed as a function of aeration rate (1, 2, 4, and 8 L/min) to obtain the optimal aeration rate of MTF. According to the tests, under a hydraulic retention time (HRT) of 60 min, the SP removal rate was approximately 30% or more at an aeration rate of 1 L/min, 50% or more at an aeration rate of 2 L/min, and 65% or more at an aeration rate of 4 L/min (Figure 6). At an aeration rate of 8 L/min, the SP removal rate was similar to that at 4 L/min. The SP removal rate also increased with increasing aeration rate under other HRT conditions; however, the rate of SP removal increase slowed at aeration rates above 4 L/min. A previous study suggested that this phenomenon was due to the SP floc becoming separated from the mesh tube media and being redistributed into the water at a high aeration rate of 4 L/min or more [10]. In addition, the higher the aeration rate, the higher the flux of air bubbles in the MTF, which eventually breaks the SP floc into smaller pieces, reducing the ability of MTF to remove SPs. The same study determined the optimal aeration rate of a bench-scale MTF as approximately 3 L/min [10], whereas this study obtained an optimal aeration rate of approximately 4 L/min.

Bench-scale MTF and PFB reactors were manufactured using poly (methyl methacrylate) (PMMA) material and operated to analyze the filter performance as a function of inflow rate and influent SP concentration using artificial seawater with added kaolin particles as the influent water. Kaolin (also called kaolinite) is a clay mineral used to make ceramics. Its chemical composition is $Al_2Si_2O_5(OH)_4$, and it is currently used for industrial purposes. Kaolin particles exhibit physical properties very similar to fine suspended particles existing in natural waters such as rivers and seas and have been widely used in studies of SP transport of fluids and studies of SP aggregation in water [27–29]. After the start

of reactor operation, the turbidity of the treated water (M-7 and P-9) was measured to observe the performance stabilization of MTF and PFB, and the total SP (TSS) of sampled water from each pot (M-2, M-3, M-4, M-5, M-6, P-2, P-3, P-4, P-5, P-6, P-7, and P-8) was measured to analyze the performance of the filters in the stable phase. The number and position of each pot of MTF and PFB are shown in Figure 3. The SP removal rate of MTF and PFB as a function of the flow rate (denoted as HRT in Figure 7) shows that the SP removal rate of PFB was superior to that of MTF (Figure 7a,b). At an HRT of 15, 20, 30, and 60 min, the SP removal rates were 32.5 ± 3.3%, 42.6 ± 4.1%, 54.8 ± 4.9%, and 64.4 ± 3.6% for MTF and 46.7 ± 3.7%, 68.0 ± 3.4%, 67.6 ± 5.1%, and 68.4 ± 3.6% for PFB, respectively. Thus, there was no significant difference in the SP removal rate of PFB between HRT values of 20 min and 60 min. Currently, the HRT operating conditions and hydraulic loading rates of DAF are 15–20 min [30] and 15–30 m/h [31], respectively. As the bench-scale PFB exhibited excellent removal performance at 20 min of HRT and the hydraulic loading rate of field MTF facilities used in actual wastewater treatment plants (Ilsan Water Restoration Center, Goyang-si, Gyeonggi-do, Republic of Korea) is 20–30 m/h (maximum loading rate: 51 m/h), this suggests that PFB facilities can compete with DAF facilities if they show stable performance in field experiments. In addition, the size of micro-air bubbles generated in DAF is 40–100 μm, which cannot easily remove SPs smaller than 20 μm. Therefore, the size of the SP must be aggregated to 40 μm or greater through administration of sufficient coagulant [30–32]. Previous studies have indicated that the microalgae removal efficiency of MTF is better than that of DAF under the same coagulant injection conditions [10], and that SP particle sizes of 10 μm and 20 μm are effectively removed by a mesh tube media column without coagulant [9]. This suggests that PFB using mesh tube media can respond more effectively than DAF when microalgal cells (smaller than 20 μm) induce harmful algal bloom conditions. However, field experiments using field-scale PFB and DAF facilities under high-concentration harmful algal bloom conditions are required to verify this hypothesis. In addition, field experiments to remove oil droplets in wastewater treatment are also considered to be meaningful.

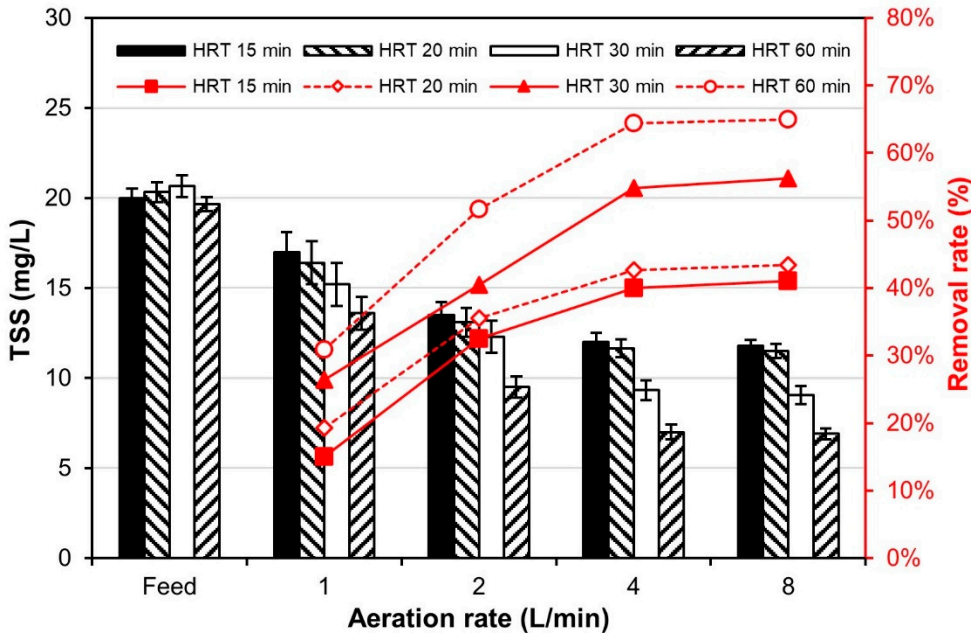

Figure 6. Suspended particle (SP) removal efficiency of the bench-scale MTF reactor as a function of aeration rate.

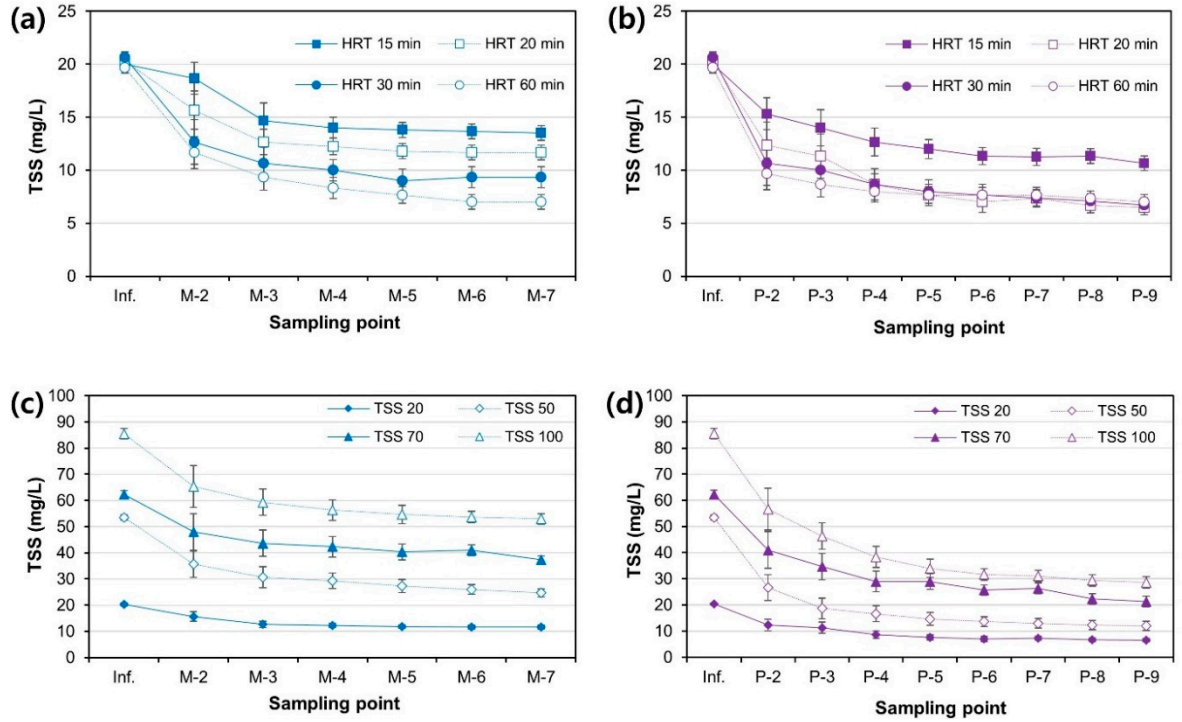

Figure 7. SP concentration at each port of the bench-scale MTF and PFB reactors as a function of influent flow rate and SP concentration: (**a**) total suspended solids (TSS) of MTF (flow rate conditions); (**b**) TSS of PFB (flow rate conditions); (**c**) TSS of MTF (TSS concentration conditions), and (**d**) TSS of PFB (TSS concentration conditions). Each sample was analyzed three times to derive the data reliability and standard deviation.

According to the experiment that varied the SP concentration in the influent (denoted as TSS in Figure 7), PFB showed better SP removal performance than MTF (Figure 7c,d). The SP removal rates under 20, 50, 70, and 100 mg/L of initial TSS were 42.6%, 53.9%, 40.1%, and 38.0% for MTF but 68.0%, 77.6%, 65.8%, and 66.4% for PFB, respectively. Both MTF and PFB showed the best SP removal performance under the condition of 50 mg/L of initial TSS (at a fixed HRT of 20 min). In MTF, the TSS concentration decreased rapidly from the influent to M-3, then more gradually from M-4 to M-7 (Figure 7c). Similarly, in PFB, the TSS concentration decreased rapidly from the influent to P-5, then more gradually from P-6 to P-9 (Figure 7d). This is because the SP removal efficiency differs in each compartment of the filter bed within the same reactor. Wegelin suggested the following simple equation for determining the efficiency of SP removal in each compartment (Equation (8)) [5,11]:

$$C_e = C_0 E_1^* E_2^* E_3^* \ldots E_n^* \quad (8)$$

where C_0 is the SP concentration of the roughing filter influent, Ce is the SP concentration of the roughing filter effluent, and E_1, E_2, E_3, ... , E_n is the filtration efficiency of each compartment (1, 2, 3 respectively), where $E_1 = 1 - E_1^*$, $E_2 = 1 - E_2^*$, $E_3 = 1 - E_3^*$, ... $E_n = 1 - E_n^*$.

According to Figure 7c, E_1 (filtration efficiency of the M-2 compartment) at an SP concentration of 20, 50, 70, and 100 mg/L was 15.2%, 42.7%, 31.0%, and 30.6%, respectively. The average filtration efficiency of E_2 to E_6 was 8.0%, 9.1%, 2.7%, and 1.0%, respectively. This indicates that the filtration efficiency of the second, third, and fourth filter compartments of MTF is very poor compared to that of the first filter compartment and that SPs are not effectively circulated throughout the filter bed of MTF. According to Figure 7d, the average filtration efficiency of E_1 to E_3 at an SP concentration of 20, 50, 70, and 100 mg/L was 16.2%, 30.3%, 21.1%, and 22.4%, respectively; however, the average filtration efficiency of E_4 to E_8 was 3.2%, 1.4%, 5.7%, and 5.6%, respectively. Thus, the PFB effectively

removed SPs from P-2 to P-4, which is the down-flow compartment of PFB, and deposited the SPs more evenly on the mesh tube media than MTF. Both MTF and PFB have lower filter efficiency in the rear filter compartment than the first filter compartment. These results are related to the characteristics of the mesh tube filter media. The deposition of SPs on the media in the mesh tube filter is the main removal mechanism of the SPs [9]. The larger the size of the SPs, the more effectively the particles are deposited on the filter media because they are affected by gravity, and the electrical attraction between the particles and the filter medium increases [9]. So, relatively large SPs are removed on the first filter compartment, and the remaining small particles are not effectively removed on the rear filter compartment, resulting in poor performance in the part. In Figure 8c, the size of the discharged SPs is very small compared to the deposited particles or precipitated particles, which supports this deduction. And the difference in the SP removal performance of MTF and PFB as a function of the influent flow rate of the filter or the concentration of SPs can be explained by this deduction. The higher the filter influent flow rate and the higher the influent SP concentration, the lower the filters' performance because relatively small particles of the SPs are not effectively removed in the mesh tube filter media. And the description suggests that relatively small SPs must be effectively removed by slowing down the fluid passing through the mesh tube media and making the filter media in the rear filter compartment dense (reducing the porosity) to improve the performance of MTF or PFB.

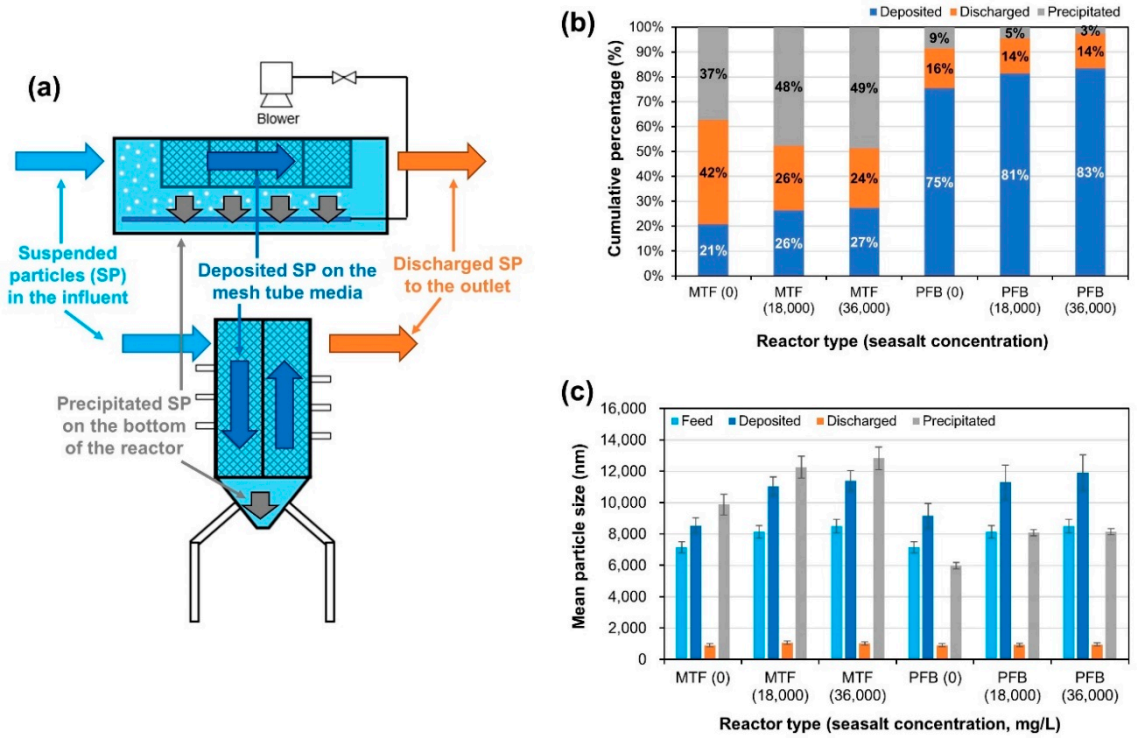

Figure 8. SP mass balance of bench-scale MTF and PFB reactors as a function of ionic concentration (artificial sea salt concentration: 0, 18,000, and 36,000 mg/L): (**a**) schematic diagram of mass balance; (**b**) deposited/discharged/precipitated particle ratio under each condition; (**c**) mean SP sizes under each condition.

The comparison of SP removal performance between MTF and PFB confirms that PFB was superior as it deposited SPs more evenly on the mesh tube media than MTF. The fate of SPs injected into MTF and PFB reactors was divided into three categories: particles deposited on the surface of the mesh tube media, particles precipitated on the bottom of the reactor tank, and particles flowing out of the reactor tank through the outlet (Figure 8a and Equation (9)):

$$SP_T = SP_{dm} + SP_P + SP_{do} \quad (9)$$

Here, SP_T is the total SPs, SP_{dm} is the SPs deposited on the mesh tube media, SP_p is the SPs precipitated at the bottom of reactor, and SP_{do} is the SPs discharged to the outlet. In order to analyze the mechanism of SP removal by MTF and PFB reactors, the deposition/discharge/precipitation ratio was analyzed by operating MTF and PFB for 2 h then measuring the SP concentration in the mesh tube media, effluent, and water remaining in the reactor (Figure 8b) (TSS concentration = 20 mg/L, HRT = 20 min). Moreover, in order to compare the fate of SPs as a function of the ion concentration of the influent, the experiment was performed under influent ion concentrations of almost 0 mg/L (DI water), approximately 18,000 mg/L (half the concentration of artificial seawater), and approximately 36,000 mg/L (the concentration of artificial seawater). The experimental results indicate that MTF predominantly removed SPs by precipitation, whereas PFB predominantly removed SPs by deposition on mesh tube media. In addition, SP deposition increased significantly with an increase of influent ion concentration from almost 0 mg/L to approximately 18,000 mg/L in both MTF and PFB. This is presumably caused by an increase in electrical attraction between the filter media and SPs. In order to analyze the electrical attraction between the SPs and filter media, zeta potential measurements of the SPs and filter media are required, along with SP size measurements; this electrical attraction is expressed by the DLVO interaction energy. For MTF and PFB, the deposition/discharge/precipitation ratio was similar under influent ion concentrations of approximately 18,000 mg/L and 36,000 mg/L, which may be because there was no significant difference in DLVO interaction energy between SP and filter media at these ion concentrations.

To analyze the fate of SP according to their characteristics, SP size was measured according to the deposition/discharge/precipitation conditions (Figure 8c). Large SPs were predominantly removed by precipitation in the MTF reactor and by deposition in the PFB reactor. At an ion concentration of almost 0 mg/L and approximately 18,000 mg/L, the size of precipitated particles in MTF and deposited particles in PFB increased significantly. The size of SPs in brackish water (ion concentration of approximately 18,000 mg/L) is larger than that in fresh water because high ionic strength promotes the aggregation of SPs. In the condition of low ion concentration, the repulsive double-layer force acts strongly and slows the aggregation rate of particles. In the condition of high ion concentration, double-layer forces are weakened, and attractive van der Waals forces induce fast aggregation; this behavior has been thoroughly explained by previous studies [33–37]. Similar to the change in the SP deposition/discharge/precipitation ratio according to ion concentration, there was little difference in the size of SPs between ion concentrations of approximately 18,000 mg/L and 36,000 mg/L.

The major factor in which suspended particles are deposited on the surface of the filter medium is the electrical attraction (e.g., van der Waals forces) between the filter medium and the suspended particles. And this electrical attraction can be calculated from the zeta potential of the suspended particles and the filter medium. Therefore, it is essential to analyze the zeta potential of the SP and filter media to infer the effect of the particles' electrical properties on deposition. Figure 9a shows the zeta potential of each particle under freshwater (TDS: 0 mg/L), brackish water (TDS: 18,000 mg/L), and artificial seawater (TDS: 36,000 mg/L) conditions. The high ionic strength of artificial seawater affects the zeta potential of not only SPs but also LDPE (the mesh tube media material) (Figure 9a). The zeta potential of the LDPE sheet was −33.13 mV in freshwater, but became positive (68.83 mV) under artificial seawater conditions. The electrical interaction between the SPs and porous filter media was analyzed using the particle size, zeta potential of the filter media and SP, and DLVO interaction energy (Figure 9). The equations for DLVO interaction energy are shown in Equations (1)–(4).

The DLVO interaction energy results show that the energy barrier of the interaction energy graph under freshwater conditions tends to increase with increasing SP sizes. With a particle size of 10 μm or more, the energy barrier was clear and stable. However, in seawater conditions, the energy barrier was removed under all conditions, causing aggregation; the DLVO interaction energy graph shows that the electrical attraction between the SP and the mesh tube medium increases as the suspended particles' size increases. In addition, the DLVO interaction energy graph under brackish water conditions at 18,000 mg/L of TDS was very similar to that under seawater conditions (TDS:

36,000 mg/L), which indicates that electrical attraction between the SP and mesh tube media is as strong in brackish water conditions as in seawater conditions.

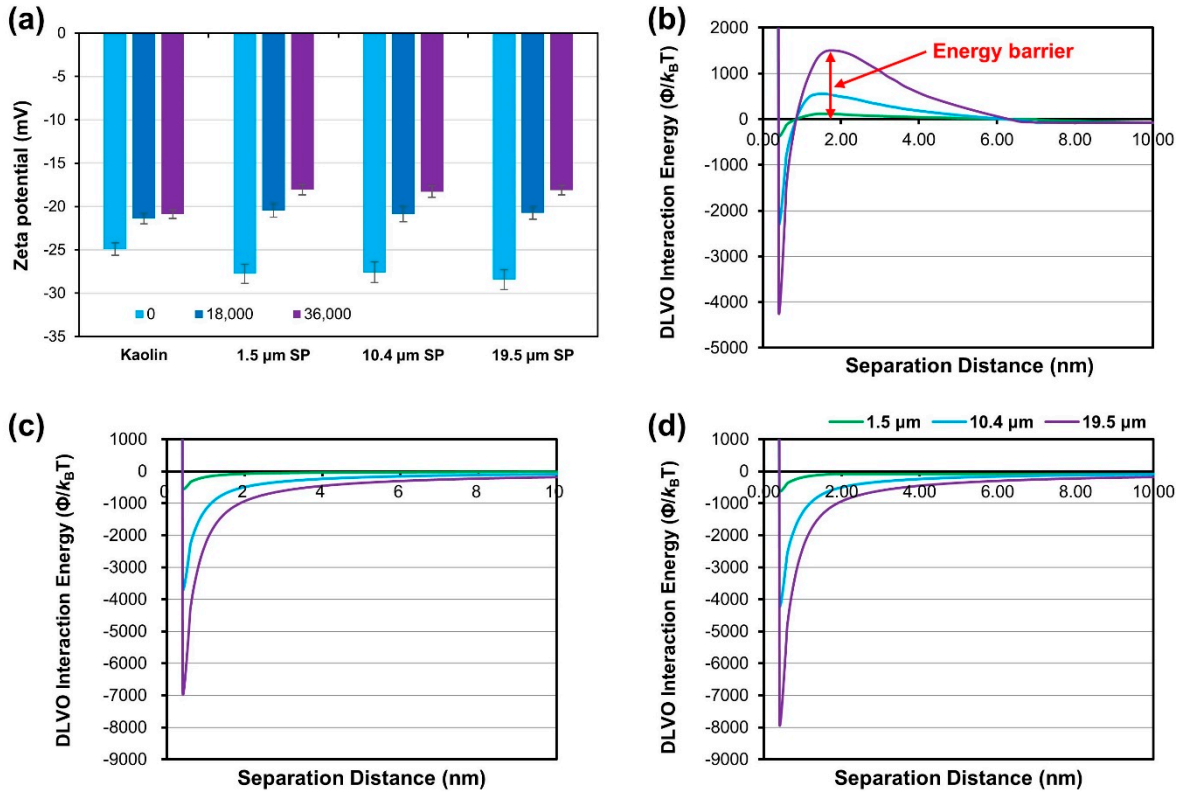

Figure 9. Zeta potential of SP and Derjaguin, Landau, Verwey, and Overbeek (DLVO) interaction energy curves between filter media material and SP: (**a**) zeta potential of SP; (**b**) DLVO interaction energy curves for an ion concentration of 0 mg/L; (**c**) 18,000 mg/L; and (**d**) 36,000 mg/L.

These data confirm that PFB showed superior SP removal performance to that of MTF. However, in order to improve the economic efficiency of actual plants, both the filter performance and energy consumption of the filter should be lower than those in the conventional primary pretreatment process. Thus, Equation (10) was used to analyze the energy consumption of MTF and PFB by obtaining the energy consumption of the fluid pump [10,38]:

$$Pw = \frac{Q\rho gh}{\eta 3.60 \times 10^6} \quad (10)$$

where Pw is the daily power consumption (kW), Q is the recycling water flow rate depending on the recycle rate (m^3/d), ρ is the water density (1000 kg/m^3), g is a gravitational constant (9.81 m/s^2), h is the pressure drop depending on the saturation pressure (m head), and η is the pump efficiency, which is assumed to be 70%. Dividing the Pw value by 24 (h) gives the energy consumption per hour (kWh), which, when divided by the water production quantity (m^3/h), gives the specific energy consumption (SEC). In order to compare the SEC of DAF, MTF, and PFB, SEC data obtained by three batch DAF operation conditions [10] and pilot-scale MTF and PFB operation conditions (Table 2) are shown in Figure 10.

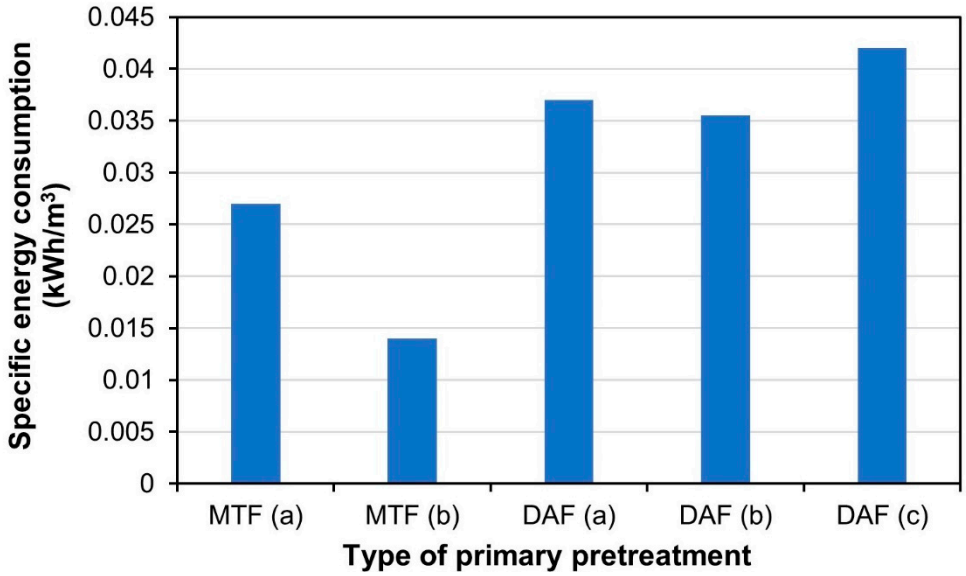

Figure 10. Comparison of specific energy consumption (SEC) of DAF and MTF. The SEC data of MTF (**b**); DAF (**a**); DAF (**b**), and DAF (**c**) were from Cha et al. 2020 [10].

The most considerable portion of DAF's energy consumption is the blower device that supplies air to the air diffuser, and the energy consumption required to generate air bubbles is determined by the saturator pressure and recycle rate [31]. In order to create microscopic air bubbles measuring several hundreds of microns, air pressure must be supplied to the air diffuser with microscopic holes, which leads to a large energy loss. Moreover, energy loss from the DAF air diffuser has yet to be substantially mitigated [31] and the SEC of DAF in the field ranges from 0.05 to 0.075 kWh/m^3 [39]. Similarly, in the work of Cha et al., the SEC of batch DAF experiments ranged from 0.035 to 0.047 kWh/m^3 [10] (Figure 10). The pressure drop of the pilot-scale MTF and PFB was analyzed through computational fluid dynamics (CFD), and the operating conditions of CFD analysis are shown in Table 2. The SEC of pilot-scale MTF, which was calculated by assuming that the MTF generates aeration using an air blower that outputs 50 L/min at an energy consumption of approximately 40 W, was 0.027 kWh/m^3 (MTF (a) in Figure 10). This is because the energy consumption of the fluid pump was minimal due to the very low head loss of 5072.53 Pa; the energy consumption of aeration required for MTF operation accounted for the majority of the total energy consumption. Therefore, if the MTF design were optimized by enlarging the process and improving the energy distribution of the diffuser, the SEC of the MTF would be significantly reduced. According to Cha et al., the SEC of MTF was calculated by assuming that the water treatment capacity of MTF was 2950 m^3/d on the 26.67 m^3 scale (61% of the total volume of the MTF reactor), which resulted in an SEC value of 0.014 kWh/m^3 (MTF (b) in Figure 10) During the wastewater treatment process using activated sludge or the membrane bio reactor (MBR) process, aeration requires more energy than water transfer using pumps. In Italian and Chinese wastewater treatment studies using activated sludge, the proportion of aeration of the total energy consumption was 50.34% and 51.38%, respectively [40,41], whereas the MBR process exhibited an energy consumption rate of aeration of 36–68% [42]. Therefore, as the aeration energy consumption of the water treatment process accounts for a major proportion of the total energy consumption, energy consumption can be greatly reduced by using processes that do not require aeration such as PFB. As expected, the SEC of PFB was significantly reduced to almost zero (0.000003 kWh/m^3). Unlike MTF, PFB exhibited a pressure drop of 9.476 Pa, resulting in very low energy head loss and very low SEC because energy was only consumed to supply influent water using the fluid pump. However, this value is a very theoretical figure and it does not mean that actual PFB reactors consume very little energy. This result means that the PFB hardly loads the fluid pump during operation, but requires the minimum amount of energy to supply sufficient influent water to the PFB pretreatment facility. In the study of

Cha et al., microalgal cell removal and turbidity removal rates were greater than 90% under the four pretreatment conditions of DAF (a), DAF (b), DAF (c), and MTF [10]. MTF used less energy than DAF and showed similar microalgal cell removal performance to DAF; however, MTF incurred the cost of replacing the mesh tube media in the filter cage (8037.5 South Korea Won, KRW/day), which was similar to the energy consumption cost of MTF (8119.6 KRW/day). The results of this study suggest that if PFB is used as pretreatment for seawater desalination, the SEC of the pretreatment can be significantly reduced compared to that of the conventional MTF or DAF, thereby significantly reducing the operating expenditure of the desalination plant.

3.3. Comparison of Filter Performance and Contamination Characteristics of MTF and PFB Field Experiments Using Blended Wastewater–Seawater Influent

Laboratory-scale experiments using artificial seawater and kaolin particles confirmed that PFB removed SP more effectively than MTF and showed better SP removal performance at an ion concentration above 18,000 mg/L than when the ion concentration was almost zero. However, laboratory-scale experiments have limited influent capacity, making it difficult to increase the operating time. Therefore, field experiments were conducted at Yeosu wastewater treatment plant (Yeosu-si, Jeollanam-do, Republic of Korea) to analyze the SP removal characteristics and organic pollutants during more than 72 h of MTF and PFB operation. To analyze whether MTF and PFB effectively remove organic SP under high ion concentration conditions, the influent was set to a 1:1 blended solution with secondary treated wastewater from the Yeosu wastewater treatment plant and natural seawater drawn from the shore next to the plant. The influent water temperature was 15–17.5 °C, the pH was 7.5, and the TDS was approximately 17,000 mg/L (Figure 4). In addition, as the TSS of the influent was very low, kaolin particles were periodically administered to maintain the TSS concentration of the influent at 20 mg/L to analyze the performance of SP in MTF and PFB. In the seawater desalination process, the process using influent water mixed with secondary treated wastewater and seawater meets the global trend of water reuse and has several advantages: (1) seawater intake and discharge requirements are reduced, (2) second-pass RO for boron control is no longer required, (3) energy consumption is reduced, (4) seawater and treated wastewater constituents are diluted in the brine to be disposed (5) the land footprint is reduced, and (6) pumping volumes are decreased [43,44]. However, the water reuse process that mixes wastewater and seawater has a high risk of causing fouling in the water treatment process due to the high concentration of SP and organic particles contained in the wastewater; another disadvantage is that it cannot be used as drinking water due to environmental regulations in many countries [44].

According to the field experiment results conducted at a HRT of 20 min, PFB showed better SP removal performance than MTF, which was similar to the laboratory-scale experiments (Figure 11). MTF maintained an SP removal rate of approximately 47% for approximately 40 h of operation before it rapidly decreased; however, PFB maintained an SP removal rate of 60% throughout the 72 h of operation. Backwashing (clean-in-place) using air scouring was performed 72 h after the start of operation, which resulted in the rapid recovery of the filter performance of PFB, which showed stable performance throughout operation. The PFB facility stably removed SP from influent water with an SP concentration of 20 mg/L without using coagulant (with a removal rate of approximately 60%).

The surface of the mesh tube media was photographed with a low-vacuum scanning electron microscopy (LV-SEM) to compare the pristine mesh tube media with contaminated media and media washed by backwashing to visually observe the contamination and cleaning properties of the mesh tube media (Figure 12). As described in the materials and methods part, the mesh tube is composed of a lattice structure made of LDPE that contains four strands of synthetic yarn to support the polyethylene lattice during the mesh tube manufacturing process. The polyethylene string constituting the lattice structure of the mesh tube media has a relatively thick and smooth surface, and the synthetic yarn has a rough surface with a thick thread intertwined with fine threads. It is predicted that a lot of SP will be deposited on the synthetic yarn due to its more complex surface structure than the LDPE string;

however, the LV-SEM observations indicate the opposite. The surface of the fouled mesh tube media reveals many SPs attached to the simpler structure of the LDPE string than the synthetic yarn. This can be explained by the aforementioned theory of DLVO interaction energy, whereby LDPE encourages the effective deposition of negatively charged SPs by converting the zeta potential into a positive charge at high ion concentrations. In addition, as the SPs adhering to the smooth surface are effectively separated from the surface of the mesh tube media during backwashing, this characteristic is expected to facilitate maintenance of the mesh tube media filter.

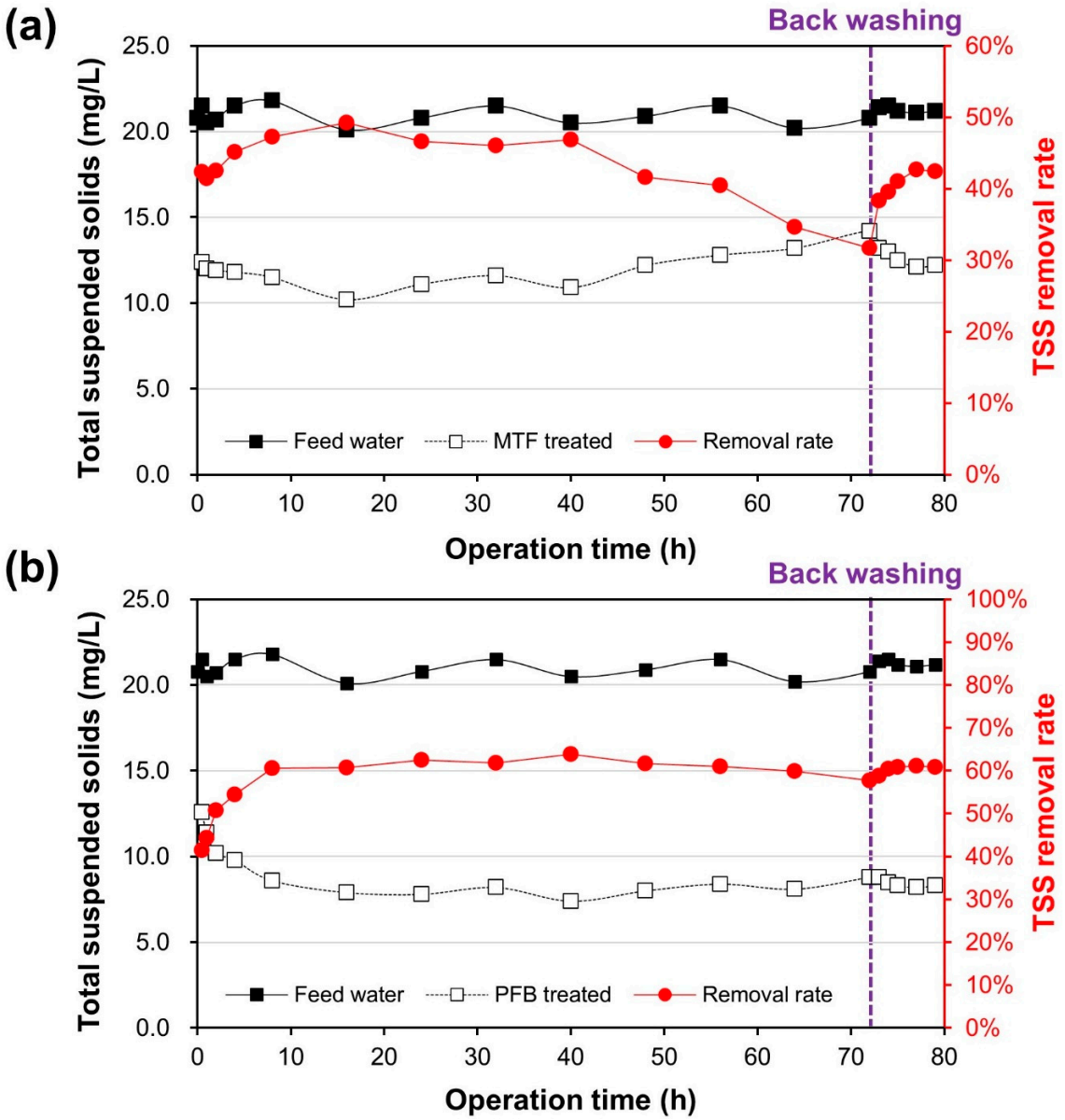

Figure 11. SP removal performance of MTF and PFB in a wastewater-seawater mixture: (**a**) TSS removal rate of MTF and (**b**) TSS removal rate of PFB.

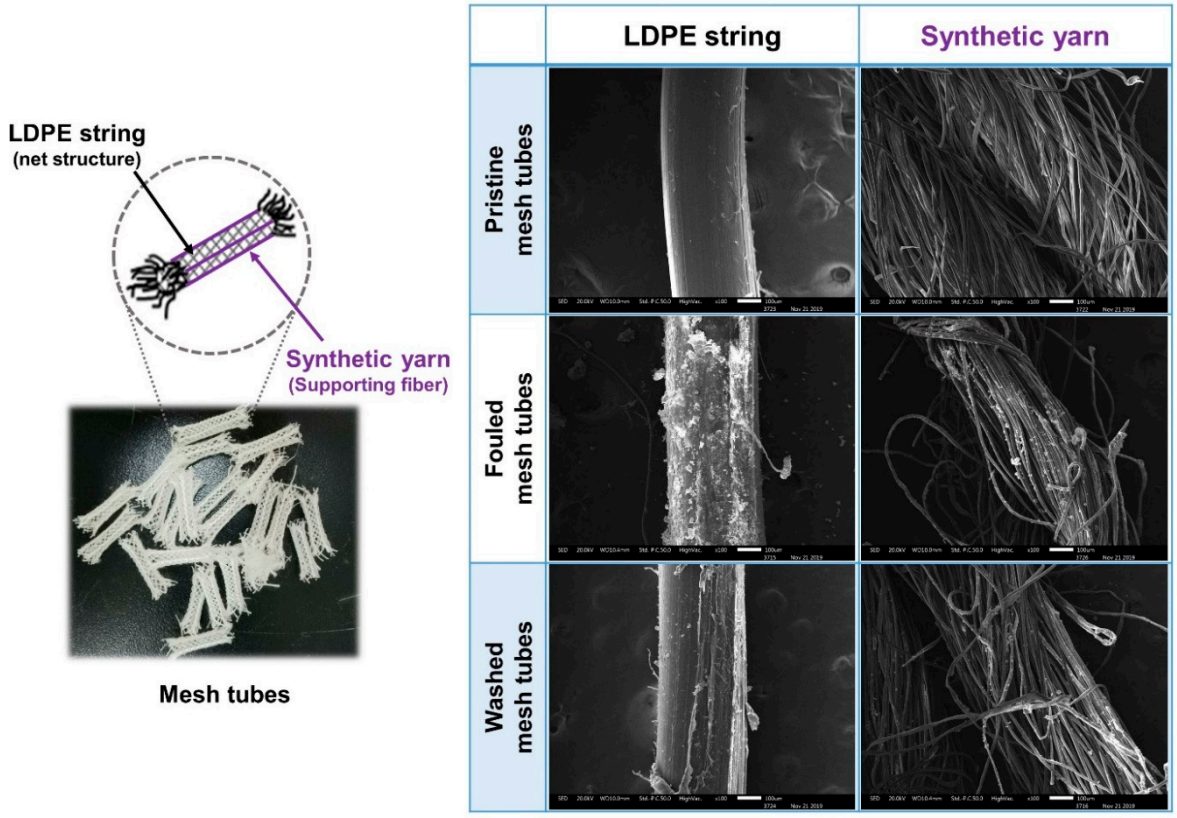

Figure 12. LV-SEM image of contaminated and washed surfaces of LDPE string and synthetic yarn.

LC–OCD was used to analyze the characteristics of organic pollutants contained in the influent, MTF-treated water, and PFB-treated water, as well as organic pollutants deposited on the surface of the mesh tube media (Figure 13). LC–OCD can calculate the hydrophobicity ratio of organic SPs and the ratio of each fraction of pollutants. The hydrophobic ratio was 6% and the hydrophilic ratio was 94% in secondary treated wastewater of the Yeosu wastewater treatment plant, whereas the hydrophilic ratio was 100% in the seawater intake from Yeosu seashore (Figure 13a). Blended wastewater–seawater influent had a hydrophobicity ratio of 5% and a hydrophilicity ratio of 95%, with no difference in the hydrophobicity/hydrophilicity ratio between the influent water and the treated water of MTF and PFB. However, in order to analyze the characteristics of organic contaminants deposited on the mesh tube media, the rinsed water of both MTF and PFB was analyzed using LC–OCD, revealing hydrophobicity of 12% and hydrophilicity of 88%. The hydrophobicity ratio of the organic SP attached to the mesh tube media increased from that of the SP in the influent because the hydrophobic biopolymer was more effectively attached to the polyethylene mesh tube media than the hydrophilic biopolymer (Figure 13b).

In Figure 13b, the ratio of each fraction of organic pollutants analyzed by LC–OCD is displayed as cumulative ratio bar graphs. Low-molecular-weight (LMW) acids were hardly detected in the secondary treated wastewater, and biopolymers were detected at low concentrations (55 μg/L, 6.2%) in Yeosu seawater. LMW acids have a particle size of 350 Dalton (Da) or less and the lowest percentage of LC–OCD fractions in natural seawater [45]. Due to the very small particle size of LMW acids, the removal rate was approximately 10% in the dual media filtration (DMF) process, approximately 5% in the ultra-filtration (UF) process, and 55% in the reverse osmosis (RO) process [45]. Biopolymers have a particle size of 20,000 Da or more and are the largest particulate substances in the LC–OCD fraction, including polysaccharides and proteins [45]. Polysaccharides and proteins contained in surface water are known to contribute to UF membrane fouling [46,47], as well as irreversible fouling of coarse membranes with a pore size of 750 kDa [46,48]. LC–OCD analysis did not reveal a significant difference between mixed wastewater–seawater influent, MTF-treated water, and PFB-treated water (Figure 13b).

As the mesh tube media of MTF and PFB cannot effectively remove organic fine SPs, a secondary pretreatment process such as multi-media filtration (MMF), or a cartridge filter process is required to protect the membranes of downstream micro filtration (MF), UF, and RO systems from organic fine-particle fouling.

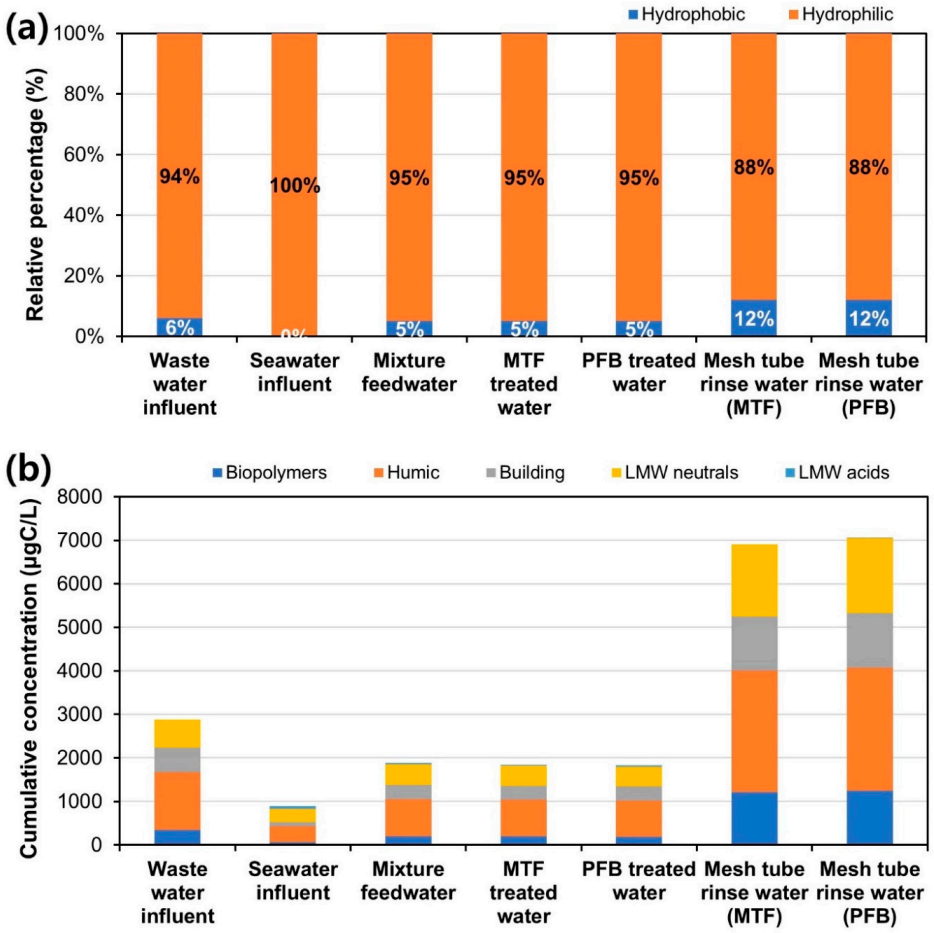

Figure 13. Liquid chromatography–organic carbon detection (LC–OCD) analysis of the wastewater–seawater mixture experiments: (**a**) hydrophobic/hydrophilic ratio of suspended organic particles and (**b**) composition ratio of suspended organic particles.

In order to analyze the fraction of organic SPs attached to the mesh tube media, the rinsed water of MTF and PFB was analyzed by LC–OCD. The proportion of biopolymer deposited on the mesh tube media was 17.6%, and the proportion of humic acid deposited on the mesh tube media was 40.5% (Figure 13b). Humic acids have a particle size of less than 1000 Da and are hard to remove during pretreatment processes such as DMF due to their small molecular weight [45], which are known to cause serious fouling of nano-filtration (NF) membranes in the presence of calcium ions [49,50]. The mesh tube media exhibited a relatively weak ability to deposit humic acids but an excellent ability to deposit biopolymers. This seems to be the cause of the increase in hydrophobicity of the mesh tube rinsed water from that of the wastewater-seawater mixed influent, as mentioned above (Figure 13a). The organic-SP removal properties of the mesh tube media filters revealed in this study may be helpful for designing seawater desalination plants.

4. Conclusions

In this study, we presented an improved MTF design based on a PFB, which exhibited superior SP removal performance to conventional MTF. We then compared the applicability of MTF and PFB to the

primary pretreatment process for seawater desalination and the water reuse process. The primary findings from this study are summarized as follows:

- In experiments to remove SPs using bench-scale MTF and PFB reactors, PFB exhibited better SP removal performance than MTF under various HRT and TSS conditions. At an HRT of 15, 20, 30, and 60 min, the SP removal rates for MTF were 32.5%, 42.6%, 54.8%, and 64.4%, respectively, whereas those for PFB were 46.7%, 68.0%, 67.6%, and 68.4%, respectively.
- The fate of SPs injected into MTF and PFB reactors was divided into three categories: particles deposited on the surface of the mesh tube media, particles precipitated on the bottom of the reactor tank, and particles flowing out of the reactor tank through the outlet. MTF predominantly removed SPs by precipitation, whereas PFB predominantly removed SPs by deposition of mesh tube media. The fate of SPs was also affected by the ion concentration in the water.
- In the extended performance analysis of a 72 h operation using blended influent water comprising natural seawater and secondary treated wastewater, PFB again showed better and more stable SP removal performance than MTF. Moreover, air scouring-based backwashing effectively removed SPs deposited on the mesh tube media. Although MTF and PFB have low organic-SP removal performance, relatively hydrophobic SPs were more efficiently deposited on the mesh tube due to the hydrophobicity of the mesh tube.
- The SEC of pilot-scale MTF and PFB experiments was 0.027 kWh/m^3 and minimum energy for influent supply, respectively, and these values are lower than the known SEC range of the field DAF (0.050 to 0.075 kWh/m^3). In the water treatment process using aeration, the proportion of energy consumed by the air blower is very large. As PFB omits aeration, the energy consumption was greatly reduced. These findings suggest that PFB is a valid alternative primary pretreatment process to DAF.

In order to verify the applicability of PFB, a pilot-scale PFB was produced as a further study, and it is necessary to compare the performance with the pilot-scale DAF and MTF process. If the pilot-scale PFB process is operated using natural seawater or wastewater, it is expected that high-concentration SPs of the influent can be removed more effectively than other primary pretreatment processes. Through the pilot-scale experiment, new problems that were not confirmed in the bench-scale experiment can be discovered, and it is considered to be an essential study to derive an improvement plan for actual plant operation.

Author Contributions: Conceptualization, D.-H.K. and I.S.K.; methodology, D.-H.K. and C.C.; software, C.C. and C.L.; validation, D.-H.K., C.C. and C.L.; formal analysis, D.-H.K.; investigation, D.-H.K., C.C., R.S.A. and H.-J.S.; resources, S.-J.A.; data curation, D.-H.K., C.L., R.S.A. and T.-T.N.; writing—original draft preparation, D.-H.K.; writing—review and editing, C.C., C.L., R.S.A., N.T. and I.S.K.; visualization, D.-H.K.; supervision, I.S.K.; project administration, I.S.K.; funding acquisition, I.S.K. All authors have read and agreed to the published version of the manuscript.

Funding: This research was funded by Korea Ministry of Environment (MOE) grant number (1485016165) And The APC was funded by Korea Ministry of Environment (MOE) (1485016165).

Acknowledgments: This work was supported by the Korea Environment Industry & Technology Institute (KEITI) through Industrial Facilities & Infrastructure Research Program, funded by Korea Ministry of Environment (MOE) (1485016165) and partly supported by GIST Research Institute (GRI) grant funded by the GIST in 2020.

Conflicts of Interest: The authors declare no conflict of interest.

References

1. Voutchkov, N. Considerations for selection of seawater filtration pretreatment system. *Desalination* **2010**, *261*, 354–364. [CrossRef]
2. Jeong, S.; Kim, S.J.; Kim, L.H.; Shin, M.S.; Vigneswaran, S.; Nguyen, T.V.; Kim, I.S. Foulant analysis of a reverse osmosis membrane used pretreated seawater. *J. Membr. Sci.* **2013**, *428*, 434–444. [CrossRef]
3. Edzwald, J.K.; Haarhoff, J. Seawater pretreatment for reverse osmosis: Chemistry, contaminants, and coagulation. *Water Res.* **2011**, *45*, 5428–5440. [CrossRef]

4. NKwonta, O. A comparison of horizontal roughing filters and vertical roughing filters in wastewater treatment using gravel as a filter media. *Int. J. Phys. Sci.* **2010**, *5*, 1240–1247.
5. Wegelin, M. *Surface Water Treatment by Roughing Filters*; Swiss Centre for Development Cooperation in Technology and Management: Duebendorf, Switzerland, 1996.
6. Marshall, H. *Environmental Nanotechnology*; ED-TECH: Essex, UK, 2018.
7. Jayalath, J.; Padmasiri, J.; Kulasooriya, S.; Jayawardena, B.; Fonseka, W.; Wijesinghe, L. Algae removal by roughing filter. In *Affordable Water Supply and Sanitation*; Water, Engineering and Development Centre: London, UK, 1994.
8. Kim, K.; Kim, I.T.; Ahn, K.H.; Park, J.H.; Lee, Y.J. Water Treatment Apparatus Having Meshed Tubes Provided with Cilia and Water Treatment Method Using the Same. U.S. Patent US8475653B2, 2 July 2013.
9. Kim, D.H.; Lee, C.; Choi, C.; Ahn, S.J.; Kim, I. Transport analysis of particulate matter in media-saturated mesh tube filter for the desalination primary pretreatment process. *Desalination* **2020**, *495*, 114642. [CrossRef]
10. Cha, G.; Choi, S.; Lee, H.; Kim, K.; Ahn, S.; Hong, S.K. Improving energy efficiency of pretreatment for seawater desalination during algal blooms using a novel meshed tube filtration process. *Desalination* **2020**, *486*, 114477. [CrossRef]
11. Nkwonta, O.; Ochieng, G. Roughing filter for water pre-treatment technology in developing countries: A review. *Int. J. Phys. Sci.* **2009**, *4*, 455–463.
12. Elimelech, M.; Gregory, J.; Jia, X. *Particle Deposition and Aggregation: Measurement, Modelling and Simulation*; Butterworth-Heinemann: Oxford, UK, 2013.
13. Bennacer, L.; Ahfir, N.D.; Alem, A.; Wang, H. Coupled effects of ionic strength, particle size, and flow velocity on transport and deposition of suspended particles in saturated porous media. *Transp. Porous Media* **2017**, *118*, 251–269. [CrossRef]
14. Redman, J.A.; Walker, S.L.; Elimelech, M. Bacterial adhesion and transport in porous media: Role of the secondary energy minimum. *Environ. Sci. Technol.* **2004**, *38*, 1777–1785. [CrossRef]
15. Frey, J.M.; Schmitz, P.; Dufrêche, J.; Pinheiro, I.G. Particle deposition in porous Media: Analysis of hydrodynamic and weak inertial effects. *Transp. Porous Media* **1999**, *37*, 25–54. [CrossRef]
16. Bhattacharjee, S.; Elimelech, M. Surface element integration: A novel technique for evaluation of DLVO interaction between a particle and a flat plate. *J. Colloid Interface Sci.* **1997**, *193*, 273–285. [CrossRef]
17. Tufenkji, N.; Elimelech, M. Correlation equation for predicting single-collector efficiency in physicochemical filtration in saturated porous media. *Environ. Sci. Technol.* **2004**, *38*, 529–536. [CrossRef]
18. Ruckenstein, E.; Prieve, D.C. Adsorption and desorption of particles and their chromatographic separation. *AIChE J.* **1976**, *22*, 276–283. [CrossRef]
19. Khilar, K.C.; Vaidya, R.; Fogler, H. Colloidally-induced fines release in porous media. *J. Pet. Sci. Eng.* **1990**, *4*, 213–221. [CrossRef]
20. Ryan, J.N.; Gschwend, P.M. Effects of ionic strength and flow rate on colloid release: Relating kinetics to intersurface potential energy. *J. Colloid Interface Sci.* **1994**, *164*, 21–34. [CrossRef]
21. Choi, C.; Lee, C.; Park, N.S.; Kim, I.S. Numerical study of fluid behavior on protruding shapes within the inlet part of pressurized membrane module using computational fluid dynamics. *Environ. Eng. Res.* **2019**, *25*, 498–505. [CrossRef]
22. Sharma, C.; Malhotra, D.; Rathore, A.S. Review of computational fluid dynamics applications in biotechnology processes. *Biotechnol. Prog.* **2012**, *27*, 1497–1510. [CrossRef] [PubMed]
23. Kavianipour, O.; Ingram, G.D.; Vuthaluru, H.B. Investigation into the effectiveness of feed spacer configurations for reverse osmosis membrane modules using Computational Fluid Dynamics. *J. Membr. Sci.* **2017**, *526*, 156–171. [CrossRef]
24. Versteeg, H.K.; Malalasekera, W. *An Introduction to Computational Fluid Dynamics: The Finite Volume Method*, 2nd ed.; Pearson Education: Essex, UK, 2007.
25. Launder, B.E.; Spalding, D.B. The numerical computation of turbulent flows. In *Numerical Prediction of Flow, Heat Transfer, Turbulence and Combustion*; Pergamon Press: New York, NY, USA, 1983; pp. 96–116.
26. Sun, F.; Xiao, K.; Zhu, W.; Withanageb, N.; Zhou, Y. Enhanced sludge solubilization and dewaterability by synergistic effects of nitrite and freezing. *Water Res.* **2018**, *130*, 208–214. [CrossRef]
27. Mathur, S. Kaolin flotation. *J. Colloid Interface Sci.* **2002**, *256*, 153–158. [CrossRef]
28. Chen, Y.; Liu, S.; Wang, G. A kinetic investigation of cationic starch adsorption and flocculation in kaolin suspension. *Chem. Eng. J.* **2007**, *133*, 325–333. [CrossRef]

29. Ho, Y.; Ismail, N.; Alkarkhi, A.F.; Morad, N. Characterization of biopolymeric flocculant (pectin) and organic synthetic flocculant (PAM): A comparative study on treatment and optimization in kaolin suspension. *Bioresour. Technol.* **2010**, *101*, 1166–1174. [CrossRef] [PubMed]
30. Voutchkov, N. *Desalination Engineering: Planning and Design*; McGraw Hill Professional: New York, NY, USA, 2012.
31. Edzwald, J.K. Dissolved air flotation and me. *Water Res.* **2010**, *44*, 2077–2106. [CrossRef]
32. Lakghomi, B.; Lawryshyn, Y.; Hofmann, R. A model of particle removal in a dissolved air flotation tank: Importance of stratified flow and bubble size. *Water Res.* **2015**, *68*, 262–272. [CrossRef]
33. López-León, T.; Jodar-Reyes, A.B.; Bastos-González, D.; Ortega-Vinuesa, J.L. Hofmeister effects in the stability and electrophoretic mobility of polystyrene latex particles. *J. Phys. Chem. B* **2003**, *107*, 5696–5708. [CrossRef]
34. Furlong, D.N.; Launikonis, A.; Sasse, W.H.F.; Sanders, J.V. Colloidal platinum sols. Preparation, characterization and stability towards salt. *J. Chem. Soc. Faraday Trans. 1 Phys. Chem. Condens. Phases* **1984**, *80*, 571–588. [CrossRef]
35. Behrens, S.H.; Borkovec, M.; Schurtenberger, P. Aggregation in charge-stabilized colloidal suspensions revisited. *Langmuir* **1998**, *14*, 1951–1954. [CrossRef]
36. Kobayashi, M.; Skarba, M.; Galletto, P.; Čakara, D.; Borkovec, M. Effects of heat treatment on the aggregation and charging of Stöber-type silica. *J. Colloid Interface Sci.* **2005**, *292*, 139–147. [CrossRef]
37. Ryde, N.; Matijević, E. Kinetics of heterocoagulation. Part 4—Evaluation of absolute coagulation rate constants using a classical light scattering technique. *J. Chem. Soc. Faraday Trans.* **1994**, *90*, 167–171. [CrossRef]
38. Ometto, F.; Pozza, C.; Whitton, R.; Smyth, B.; Torres, A.G.; Henderson, R.; Jarvis, P.; Jefferson, B.; Villa, R. The impacts of replacing air bubbles with microspheres for the clarification of algae from low cell-density culture. *Water Res.* **2014**, *53*, 168–179. [CrossRef]
39. Twort, A.C.; Ratnayaka, D.D.; Brandt, M.J. *Water Supply*; Butterworth-Heinemann: Oxford, UK, 2000.
40. Panepinto, D.; Fiore, S.; Zappone, M.; Genon, G.; Meucci, L. Evaluation of the energy efficiency of a large wastewater treatment plant in Italy. *Appl. Energy* **2016**, *161*, 404–411. [CrossRef]
41. Tao, X.; Chengwen, W. Energy consumption in wastewater treatment plants in China. In Proceedings of the World Congress on Water, Climate and Energy 2012, Dublin, Ireland, 13–18 May 2012.
42. Krzeminski, P.; Van Der Graaf, J.H.J.M.; Van Lier, J.B. Specific energy consumption of membrane bioreactor (MBR) for sewage treatment. *Water Sci. Technol.* **2012**, *65*, 380–392. [CrossRef] [PubMed]
43. Wei, X.; Binger, Z.M.; Achilli, A.; Sanders, K.T.; Childress, A.E. A modeling framework to evaluate blending of seawater and treated wastewater streams for synergistic desalination and potable reuse. *Water Res.* **2020**, *170*, 115282. [CrossRef]
44. Intelligence, G.W. *IDA Desalination Yearbook 2016–2017*; Media Analytics Ltd.: Oxford, UK, 2016.
45. Simon, F.X.; Penru, Y.; Guastalli, A.R.; Esplugas, S.; Llorens, J.; Baig, S. NOM characterization by LC-OCD in a SWRO desalination line. *Desalination Water Treat.* **2013**, *51*, 1776–1780. [CrossRef]
46. Katsoufidou, K.; Sioutopoulos, D.; Yiantsios, S.; Karabelas, A.J. UF membrane fouling by mixtures of humic acids and sodium alginate: Fouling mechanisms and reversibility. *Desalination* **2010**, *264*, 220–227. [CrossRef]
47. Jermann, D.; Pronk, W.; Meylan, S.; Boller, M. Interplay of different NOM fouling mechanisms during ultrafiltration for drinking water production. *Water Res.* **2007**, *41*, 1713–1722. [CrossRef]
48. Kimura, K.; Hane, Y.; Watanabe, Y.; Amy, G.; Ohkuma, N. Irreversible membrane fouling during ultrafiltration of surface water. *Water Res.* **2004**, *38*, 3431–3441. [CrossRef] [PubMed]
49. Beyer, M.; Lohrengel, B.; Nghiem, L.D. Membrane fouling and chemical cleaning in water recycling applications. *Desalination* **2010**, *250*, 977–981. [CrossRef]
50. Hong, S.; Elimelech, M. Chemical and physical aspects of natural organic matter (NOM) fouling of nanofiltration membranes. *J. Membr. Sci.* **1997**, *132*, 159–181. [CrossRef]

© 2020 by the authors. Licensee MDPI, Basel, Switzerland. This article is an open access article distributed under the terms and conditions of the Creative Commons Attribution (CC BY) license (http://creativecommons.org/licenses/by/4.0/).